Investigation of the temperature dependence of dielectric relaxation in liquid water by THz reflection spectroscopy and molecular dynamics simulation

Cecilie Rønne and Lars Thrane[a)]
Department of Chemistry, Aarhus University, Langelandsgade 140, DK-8000 Århus C, Denmark

Per-Olof Åstrand
Chemistry Laboratory III, H. C. Ørsted Institute, University of Copenhagen, Universitetsparken 5, DK-2100 Copenhagen Ø, Denmark

Anders Wallqvist
Frederick Cancer Research and Development Center, National Cancer Institute, Science Applications International Corporation, Frederick, Maryland 21702

Kurt V. Mikkelsen
Chemistry Laboratory III, H. C. Ørsted Institute, University of Copenhagen, Universitetsparken 5, DK-2100 Copenhagen, Ø, Denmark

Søren R. Keiding[b)]
Department of Chemistry, Aarhus University, Langelandsgade 140, DK-8000 Århus C, Denmark

(Received 19 May 1997; accepted 7 July 1997)

We report measurements of the real and imaginary part of the dielectric constant of liquid water in the far-infrared region from 0.1 to 2.0 THz in a temperature range from 271.1 to 366.7 K. The data have been obtained with the use of THz time domain reflection spectroscopy, utilizing ultrashort electromagnetic pulses generated from a photoconductive antenna driven by femtosecond laser pulses. A Debye model with an additional relaxation time is used to fit the frequency dependence of the complex dielectric constants. We obtain a fast (fs) and a Debye (ps) relaxation time for the macroscopic polarization. The corresponding time correlation functions have been calculated with molecular dynamics simulations and are compared with experimental relaxation times. The temperature dependence of the Debye relaxation time is analyzed using three models: Transition state theory, a Debye–Stoke–Einstein relation between the viscosity and the Debye time, and a model stating that its temperature dependence can be extrapolated from a singularity of liquid water at 228 K. We find an excellent agreement between experiment and the two latter models. The simulations, however, present results with too large statistical error for establishing a relation for the temperature dependence. [S0021-9606(97)50838-5]

I. INTRODUCTION

Water is in many aspects a remarkable liquid. Apart from its importance in biological processes and the extended use in chemistry as solvent, the exceptional properties of liquid water in their own justify investigations.[1–4] Although properties of liquid water have been studied for many years, the microscopic mechanisms leading to its anomalous properties are far from fully understood. This work is devoted to the study of dielectric relaxation, which previously has given valuable information about the dynamics of both liquids and solutions.[5,6] According to the simple model proposed by Debye,[7,8] a macroscopic polarization is created due to an alignment of the molecular dipole moments if an external electric field is applied to a polar liquid. Removal of the electric field cause a relaxation of the polarization as a consequence of the thermal fluctuations in the liquid. In the case of water, this simple picture is complicated by the ability of liquid water to form a highly distorted tetrahedral hydrogen-bond network. In addition, compared with other polar liquids, water is expected to have a fast dynamical behavior due to its small molecular moments of inertia.[2]

The relaxational response of liquids is found in the microwave and far-infrared region of the electromagnetic spectrum. A frequency range from 0.01 to 2 THz ($3.3–66.7\ \mathrm{cm}^{-1}$) corresponds to relaxation times from 80 fs to 16 ps (Defined as $\omega_c\tau=1$). During the last decade there has been an increasing effort to study the ultrafast response of water in this spectral region due to progress in various experimental techniques: Temperature-dependent studies of water with the use of low-frequency depolarized Raman spectroscopy (DRS) have been reported.[9,10] Mizoguchi *et al.* have been able to reproduce the observed DRS-spectrum (up to $250\ \mathrm{cm}^{-1}$) using a model including two resonance contributions (broad bands around 60 and $190\ \mathrm{cm}^{-1}$) and one relaxation process.[10] Recently, several workers have employed optical-heterodyne detected Raman-induced Kerr effect spectroscopy (OHD-RIKES/OKE)[11–13] to study the dynamics of liquid water. This is a technique where birefringence is

[a)]Permanent address: Optics and Fluid Dynamics Department, Risø National Laboratory, DK-4000 Roskilde, Denmark.
[b)]Electronic-mail: Keiding@kemi.aau.dk

induced in order to measure the nonlinear polarization. This kind of study gives two relaxation times: 0.5 ± 0.03 ps and 1.7 ± 0.3 ps at 298 K[12] as well as 0.40 and 1.16 ps at 295 K.[13] The time-dependent fluorescence Stokes shift technique (TDFSS), which is assumed to give a linear response from the solvent, have recently been improved to give a fs time resolved water measurements.[14,15] In TDFSS a suitable solute molecule is excited by a short laser pulse thereby changing the charge distribution. The subsequent reorientation of the solvent is monitored by measuring the time-dependent fluorescence. Jimenez *et al.* have measured a very fast response ($\leqslant 55$ fs) of liquid water using TDFSS.[15] Another technique giving a linear response is THz time domain spectroscopy (THz-TDS).[16,17] This is based on ultrashort electromagnetic pulses (THz pulses) which are generated and detected by small photoconductive antennas driven by fs laser pulses.[18,19] The bandwidth of the THz pulses extends from 50 GHz to several THz. The broad bandwidth, the high signal to noise ratio, and the frequency range covered make THz-pulses well suited for far-infrared spectroscopy. THz-TDS have been used in spectroscopic investigations of gases,[19] solids,[20] and liquids.[21] These experiments have all been performed as transmission experiments, but in order to study highly absorbing samples, as for example polar liquids, we have recently introduced THz-TDS in the reflection mode.[16] This experimental technique has been used in the present work to measure the complex dielectric constant of liquid water in the frequency range from 0.1 to 2 THz.

A key factor in obtaining knowledge about the structure and dynamics of a liquid is to investigate their temperature dependence. Studies of for instance density, proton mobility, and viscosity of water have turned out to be a valuable tool for testing theories about the liquid structure of water.[3,22–25] In this work, we investigate the dynamics of liquid water by measuring the temperature dependence of dielectric relaxation times, thus allowing us to obtain information about the forces responsible for the dynamics of liquid water.

Experiments provide only ensemble averages, but we would like to explain experimental data such as IR or microwave spectra in terms of molecular mechanisms. In a molecular dynamics (MD) simulation, macroscopic properties of a liquid or a solution are calculated from ensemble averages of microscopic properties of the system. The microscopic model employed in MD simulations thus provides microscopic interpretations. For the microscopic model to be valid it is, however, required that the MD simulation is able to reproduce the experimental data. It has turned out that simulations of static dielectric constants and dielectric relaxation are nontrivial from a methodological point of view and that the convergence of the sampled properties are slow.[26,27] In this work, we have performed extensive MD simulations of dielectric properties at selected temperatures corresponding to the experimental data.

II. EXPERIMENT

The THz time domain reflection spectrometer is shown in Fig. 1. A pulse from a Ti sapphire fs laser ($\lambda=800$ nm; pulse energy ~ 0.5 nJ, pulse width ~ 70 fs, repetition rate 76 MHz) is split by a beam splitter, and one part of the beam is focused onto an emitting dipole antenna[21] (inset in Fig. 1). The laser pulses generate free charge carriers, which are accelerated by biasing the antenna with 40 V. The resulting time-dependent photocurrent with subpicosecond rise time acts as source for the subpicosecond THz pulses. These are radiated into the substrate and collimated by a hyperhemispherical lens made of high resistivity silicon and a 90° off-axis paraboloidal mirror. A silicon beam splitter reflects approximately half of the THz beam onto the sample cell at normal incidence. The sample cell is equipped with a front window made of crystalline, high resistivity silicon, which has a very low dispersion and absorption in the far-infrared region.[20] The window is carefully polished to ensure parallelism and flatness. When a single THz pulse arrives at the sample cell, one part is reflected at the air–silicon interface, while another is reflected at the silicon–liquid interface. The THz beam leaving the sample cell is transmitted through the silicon beam splitter and focused onto a detecting dipole antenna (inset in Fig. 1) by a 90° off-axis paraboloidal mirror and a hyper-hemispherical silicon lens. The THz-detector is biased by the THz radiation and gated by the second part of the laser pulse that has been sent through a variable delay line. The induced photocurrent is thus proportional to the electric field of the THz pulse. The time dependence of the photocurrent is measured by scanning the delay line with a computer controlled dc motor. At each scan 2048 data points, separated by 0.04 ps, are collected with a time constant of 100 ms.

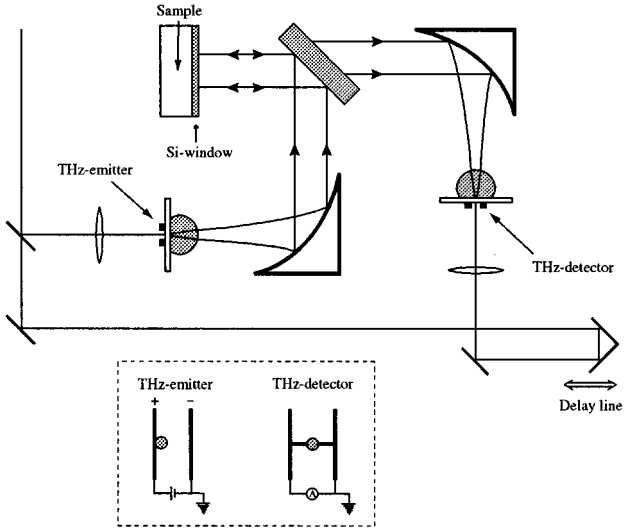

FIG. 1. THz time domain reflection spectrometer. The insets show the dipole antennas used for emission and detection of THz radiation. See Sec. II for further details.

A scan with liquid water in the sample cell is shown in Fig. 2. The first pulse in the pulse sequence is used as a reference, whereas the second pulse contains information about the complex dielectric constant of liquid water. For comparison, a scan obtained with an empty sample cell is

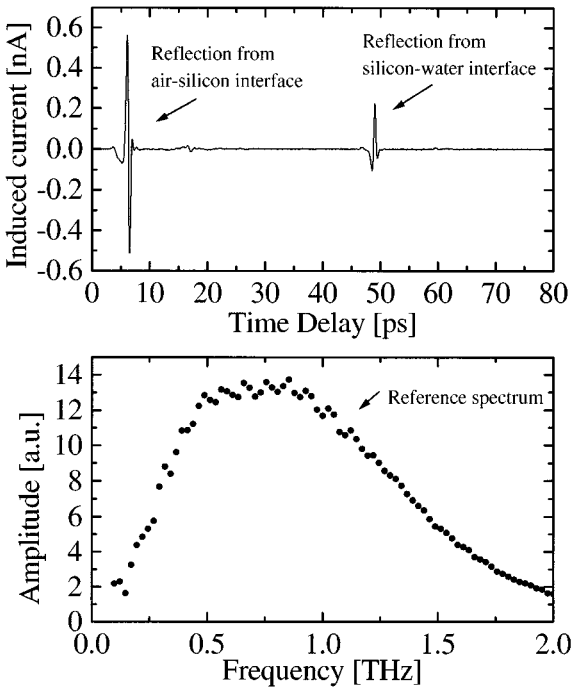

FIG. 2. Above: Pulse sequence obtained from the THz time domain reflection spectrometer with the sample cell containing three times distilled water at 315.0 K. The vertical scale is a lock-in reading with an amplification factor of 10^8 V/A. Below: The spectral amplitude of the reference pulse (the reflection from the air–silicon interface).

shown in Fig. 3. Note that the shape of the second pulse shows that water and air have different indices of refraction. The amplitude frequency spectrum of the reference pulse is also shown in Fig. 2. This spectrum illustrates the useful 2 THz bandwidth of the spectrometer.

In order to measure the properties of the liquid as a function of temperature, the sample cell is placed on a 70 W Peltier-element and insulated from the surroundings, making it possible to choose any temperature between 270 and 370 K. The temperature of the liquid is determined in the center of the sample cell by a thermocoupler, and it is made sure that the temperature is constant ($\Delta T \leqslant 0.1$ K) over the entire scan. Dry air purge is used to avoid water vapor in the setup since droplets condensing on the cold sample cell and absorption by water vapor of the THz radiation would seriously affect the results.

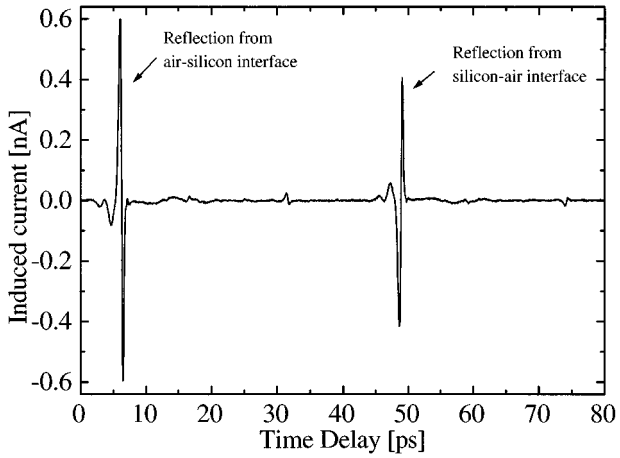

FIG. 3. Pulse sequence obtained from the THz time domain reflection spectrometer with an empty sample cell. The vertical scale is a lock-in reading with an amplification factor of 10^8 V/A.

In this work, we have also measured the refractive index of the silicon window in the frequency range from 50 GHz to 3 THz as a function of temperature. This knowledge is used in the analysis of the liquid measurements. Accordingly, the reflection spectrometer has the advantage over the transmission spectrometer[17,21] that the complex dielectric constant can be obtained from a single scan.

III. THEORY

A. Determination of the complex dielectric constant of liquid water

If a short THz pulse is reflected from the sample cell containing a liquid, the resulting pulse train consists of a pulse reflected from the front of the silicon window (reference pulse) and a delayed pulse reflected from the silicon–liquid interface (sample pulse). Measurement of the frequency-dependent change in phase and amplitude of the pulse train permits the complex dielectric constant of the liquid to be obtained from a single scan. The ratio of the Fourier transform of the reference pulse $\hat{E}_R(\nu)$ and sample pulse $\hat{E}_S(\nu)$, is

$$\frac{\hat{E}_S(\nu)}{\hat{E}_R(\nu)} = \frac{t_{\mathrm{ASi}}\hat{r}_{\mathrm{SiW}}t_{\mathrm{SiA}}}{r_{\mathrm{ASi}}} \exp\left(i\,\frac{4\pi n_{\mathrm{Si}} d_{\mathrm{Si}}\nu}{c}\right), \tag{1}$$

where t_{ASi}, t_{SiA}, r_{ASi}, and $\hat{r}_{\mathrm{SiW}}$ are the Fresnel coefficients at normal incidence for the amplitude transmission t, and reflection r. The subscripts indicate which dielectrica the interfaces consist of: air (A), silicon (Si), and water (W). The Fresnel coefficients for the air–silicon interfaces are real because dry air and silicon have no absorption. The exponential factor represents the phase shift (delay) due to propagation in the window material, where n_{Si} is the index of refraction of silicon and d_{Si} is the thickness of the silicon window. For normal incidence, the complex Fresnel reflection coefficient for the silicon–water interface is

$$\hat{r}_{\mathrm{SiW}} = (n_{\mathrm{Si}} - \hat{n}_{\mathrm{W}})/(n_{\mathrm{Si}} + \hat{n}_{\mathrm{W}}), \tag{2}$$

where $\hat{n}_{\mathrm{W}} = n_{\mathrm{W}} + i\alpha_{\mathrm{W}}c/4\pi\nu$ is the complex refractive index of water. If we express the reflection coefficient in the Euler representation, $\hat{r}_{\mathrm{SiW}} = \mathrm{R}e^{i\theta}$, and solve Eq. (2) for the unknown refractive index, n_{W} and the absorption coefficient, α_{W}, of liquid water, we obtain

$$n_{\mathrm{W}} = \frac{n_{\mathrm{Si}}(1-R^2)}{1+R^2+2R\,\cos\,\theta} \tag{3}$$

and

$$\alpha_{\mathrm{W}} = \frac{4\pi\nu n_{\mathrm{Si}}}{c}\,\frac{-2R\,\sin\,\theta}{1+R^2+2R\,\cos\,\theta}. \tag{4}$$

If both n_{Si} and d_{Si} are known, the amplitude, R, and phase angle, θ, can be determined experimentally by isolating $\hat{r}_{\mathrm{SiW}}=\mathrm{Re}^{i\theta}$ in Eq. (1). The real and imaginary parts of the dielectric constant, $\hat{\epsilon}=\epsilon'+i\epsilon''$, are calculated from the relation $\hat{\epsilon}=\hat{n}^2$. It is evident that the optical constants of water obtained from Eqs. (3) and (4) depend strongly on a precise knowledge of n_{Si} and d_{Si}. In the next section, we describe how the refractive index of silicon can be determined by measurements on an empty sample cell.

B. Determination of the refractive index of silicon

The ratio of the Fourier transform of the pulse reflected from the air–silicon interface $\hat{E}_R(\nu)$ and the pulse reflected from the silicon–air interface $\hat{E}_E(\nu)$ is given by the refractive indices of air and silicon in line with Eq. (1)

$$\frac{\hat{E}_E(\nu)}{\hat{E}_R(\nu)}=\frac{t_{\mathrm{ASi}}r_{\mathrm{SiA}}t_{\mathrm{SiA}}}{r_{\mathrm{ASi}}}\exp\left(i\,\frac{4\pi n_{\mathrm{Si}}d_{\mathrm{Si}}\nu}{c}\right), \tag{5}$$

where the real Fresnel coefficients for amplitude transmission and reflection t_{ASi}, t_{SiA}, r_{ASi}, and r_{SiA} only depend on n_{Si} and n_{A} (the index of refraction of air) for normal incidence. If we express $\hat{E}_E/\hat{E}_R$ as $R_E e^{i\theta_E}$ and make use of the fact that $(r_{\mathrm{SiA}}/r_{\mathrm{ASi}})=-1=e^{i\pi}$ at normal incidence, the unknown index of refraction of silicon, n_{Si}, can be deduced from the phase part of Eq. (5)

$$n_{\mathrm{Si}}=\frac{(\theta_E-\pi)c}{4\pi d_{\mathrm{Si}}\nu}, \tag{6}$$

while the amplitude part of Eq. (5) gives

$$n_{\mathrm{Si}}=\frac{2-R_E+2\sqrt{1-R_E}}{R_E}\,n_A. \tag{7}$$

We have obtained two equations, Eqs. (6) and (7), with two unknowns, n_{Si} and d_{Si} which gives us the possibility to determine both n_{Si} and d_{Si} from one measurement.

IV. EXPERIMENTAL RESULTS

A Determination of the frequency and temperature dependence of the refractive index of silicon

The refractive index of silicon, n_{Si}, has been determined as a function of temperature in the frequency range from 50 GHz to 3 THz. Since there is no measurable absorption in high resistivity silicon,[20] Eqs. (6) and (7) can be used. It is found that if we use Eq. (6) and a constant value for the thickness of the silicon window, $d_{\mathrm{Si}}=1.8646$ mm, we obtain the best results for the index of refraction. The linear thermal expansion coefficient of silicon is $2.616\times10^{-6}\ \mathrm{K}^{-1}$ at 300 K.[28] Within a temperature interval of 95 K the thermal expansion, Δd_{Si}, will accordingly be less than 5×10^{-4} mm and the corresponding phase shift $(2\pi n_{\mathrm{Si}}\Delta d_{\mathrm{Si}}\nu/c)$ at 1 THz is less than 4×10^{-2} rad. The thermal expansion is therefore neglected.

Measurements have been carried out in the temperature range from 275 to 304 K. The index of refraction of silicon at 295.5 K is shown in Fig. 4, which clearly demonstrates the very low dispersion of silicon in the far-infrared region. The noise at the lowest and highest frequencies is caused by the low spectral intensity of the THz pulses at these frequencies. We therefore consider n_{Si} as frequency-independent. In Fig. 5, we have plotted the value of n_{Si} at 1.0 THz as a function of temperature. Using a linear regression we obtain an equation for the temperature dependence of n_{Si} at 1.0 THz

$$n_{\mathrm{Si}}(T)=3.369\,92+(1.88\times10^{-4}\ \mathrm{K}^{-1})T, \tag{8}$$

which is shown in Fig. 5 as a full line. Because of the low dispersion this equation can be used in the analysis of the liquid measurements in the entire frequency range. Furthermore, from Eq. (8) we find the thermo-optic coefficient of silicon at 1 THz to be $\partial n_{\mathrm{Si}}/\partial T=(1.88\pm0.03)\times10^{-4}\ \mathrm{K}^{-1}$, which is in excellent agreement with a previously found value of $(1.86\pm0.08)\times10^{-4}\ \mathrm{K}^{-1}$, at 200 THz (1.5 μm).[29]

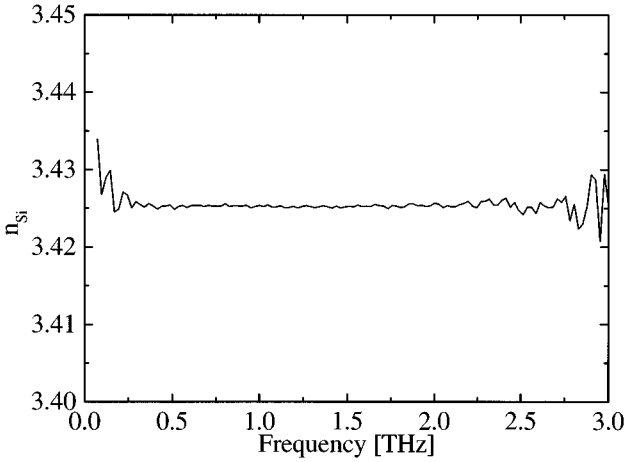

FIG. 4. A measurement of the index of refraction of silicon 295.5 K. Note the very low dispersion.

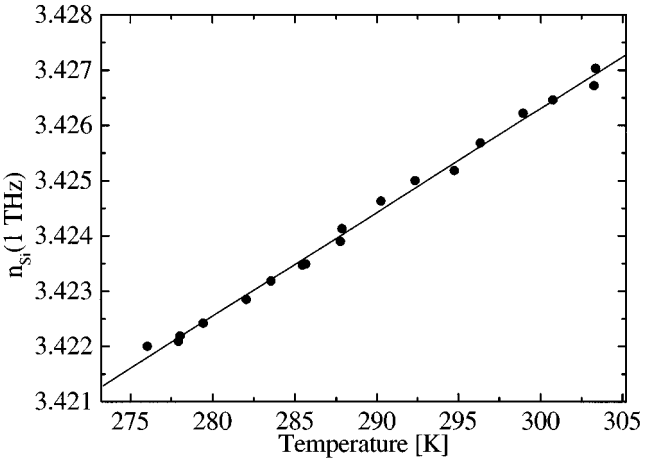

FIG. 5. The index of refraction of silicon at 1.0 THz plotted as a function of temperature. The full line is a linear fit to the points.

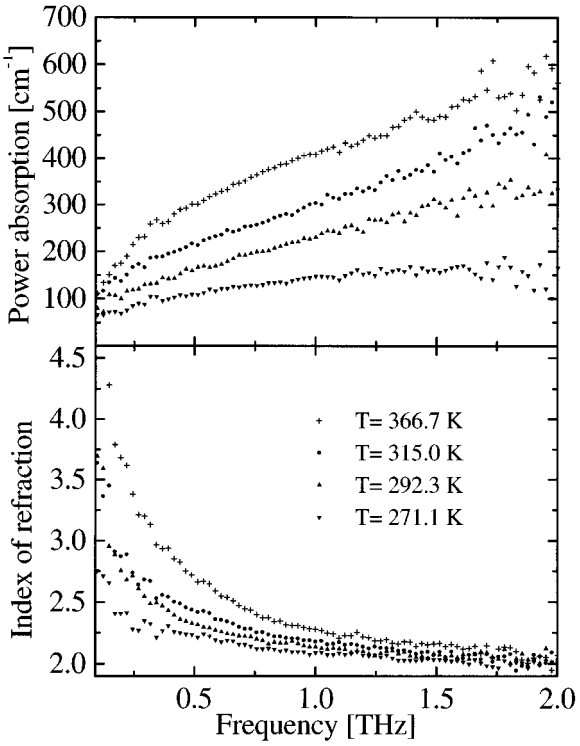

FIG. 6. The refractive index and power absorption of liquid water shown as a function of frequency at four different temperatures.

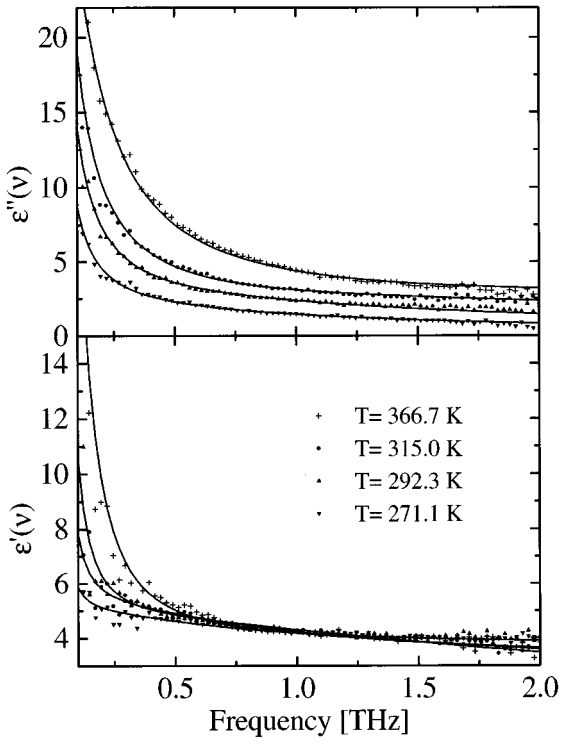

FIG. 7. The complex dielectric constant, $\hat{\epsilon}=\epsilon'+i\epsilon''$, of liquid water (points) as a function of frequency at four different temperatures. The lines show the fits to the double Debye model.

B. Determination of the complex dielectric constant of liquid water

The optical constants of liquid water have been determined as a function of temperature in the frequency range from 0.1 THz to 2 THz with the use of Eqs. (3) and (4). The measurements have been performed on three times distilled liquid water at eleven different temperatures between 271.1 and 366.7 K. The sample chamber has been flushed with water three times before the final sample is added to the cell. At temperatures up to 354.2 K, we have made four independent scans, at the highest temperature, 366.7 K, only two scans. Figure 6 shows the frequency dependence of the refractive index and power absorption obtained from averaging scans at the same temperature at four of these temperatures, including the highest and the lowest. The absorption of supercooled water (271.1 K) has an almost constant value of 100 cm^{-1} between 0.5 and 1.5 THz. The absorption at 366.7 K changes from $\sim$300 to 500 cm^{-1} in the same spectral region. For temperatures in between, the general tendency is increasing absorption with increasing frequency and temperature. The index of refraction also increases with increasing temperature but decreases with frequency. At low frequencies (0.05 THz) the index of refraction is 20% higher at 366.7 K than that at 271.1 K whereas at high frequencies only 1% higher. For data analysis we calculate the complex dielectric constant from the absorption and index of refraction. The real part, ϵ', and imaginary part, ϵ'', of the dielectric constant are shown in Fig. 7.

Absorption coefficients as high as those of liquid water make transmission experiments difficult. At room temperature, however, transmission measurements have successfully been carried out for liquid water.[17] When we compare our data at 292.2 K to room-temperature measurements in the far-infrared region of the electromagnetic spectrum, we find a good agreement.[30–32] A controversial question is the existents of a weak resonance in the frequency interval from 0.9 THz to 2.1 THz (see for example Ref. 33). The scatter in our measurements at frequencies above 1.5 THz makes it difficult to observe whether there is a shoulder on the absorption coefficient or not.

Our absorption coefficient at 331.1 K differ up to 20% from absorption coefficients reported in the far-infrared region.[30,34] We find, however, a good agreement between the index of refraction measured by us and by Zelsmann.[30] These are substantially higher than the index of refraction measured by Afsar and Hasted.[34] We also find a good agreement between our data and Zelsmann's data at 354.2 K.

In previous dielectric relaxation studies, a good agreement is found between experimental data and the Debye model, by assuming a single exponential relaxation of the polarization for frequencies up to 100 GHz.[35] If, however, the Debye model is extrapolated to THz frequencies, it fails to reproduce the experimental findings.[36] In an attempt to account for the response of water at THz frequencies, a double Debye (biexponential) model has been adopted[6,17,35,37,38]

TABLE I. Parameters from the double Debye model with the standard deviation given in parentheses. N is the number of independent scans.

T [K]	N	τ_D [ps]	τ_2 [fs]	ϵ_1	ϵ_∞
271.1	4	15.7(0.3)	220(50)	4.99(0.05)	3.8(0.2)
278.8	4	13.1(0.2)	260(50)	5.4(0.1)	3.7(0.3)
288.5	4	9.67(0.08)	180(50)	5.25(0.07)	3.4(0.2)
292.3	4	8.5(0.4)	170(40)	5.2(0.1)	3.3(0.3)
303.2	4	7.0(0.3)	200(60)	5.4(0.3)	3.4(0.3)
315.0	4	5.25(0.07)	77(9)	4.76(0.07)	2.10(0.07)
324.1	4	4.48(0.09)	72(5)	4.76(0.06)	1.6(0.2)
331.1	4	3.83(0.03)	50(10)	4.5(0.2)	⋯
343.4	4	3.26(0.08)	36(5)	4.5(0.4)	⋯
354.2	4	2.85(0.06)	51(5)	4.56(0.05)	⋯
366.7	2	2.33(0.02)	32(5)	4.1(0.1)	⋯

$$\hat{\epsilon}(\omega)=\epsilon_\infty+\frac{\epsilon_s-\epsilon_1}{1+i\omega\tau_D}+\frac{\epsilon_1-\epsilon_\infty}{1+i\omega\tau_2}. \tag{9}$$

The measured complex dielectric constant obtained from each scan has been fitted to the double Debye model with a nonlinear least-squares method.[39] The individual data points have been weighted according to the amplitude of the spectrum of the THz-pulse, giving less weight to the low- and high-frequency limits of the spectrum. We have constrained the static dielectric constant to $\epsilon_s(T)=87.91e^{-0.004\,58T[^\circ\mathrm{C}]}$ with the use of experimental data.[40] This gives us four temperature-dependent parameters: Two relaxation times, τ_D and τ_2, and two parameters that indicate the size of the coupling between the relaxation mode and the electric field, ϵ_1 and ϵ_∞. The differences $\epsilon_s-\epsilon_1$ and $\epsilon_1-\epsilon_\infty$ are accordingly relative measures of the contribution to the macroscopic polarization from the two relaxation processes. We find that within the experimental error the double Debye model given by Eq. (9) accounts for the experimental data over the entire frequency and temperature range. An alternative to adding a second relaxation process is to add a contribution from a resonance in line with Mizoguchi.[10] We find that combining a relaxation process with a damped harmonic oscillator does not give as good agreement with our data as the double Debye model.

The average value of each parameter obtained in the double Debye analysis of the N independent measurements at each temperature is reported in Table I. The numbers in parentheses are the standard deviations obtained from the averaging. Furthermore, a 1% change of ϵ_s resulted in a similar change of τ_D. The correlation between ϵ_s and τ_D will accordingly introduce an additional uncertainty to τ_D corresponding to the uncertainty of ϵ_s.

It should be noted that the fast relaxation time ($\tau_2<100$ fs) gives an almost constant contribution to the real part of Eq. (9) in the frequency range studied. Consequently, τ_2 and ϵ_∞ will be correlated and the value of ϵ_∞ remain undetermined at temperatures above 324 K owing to the limited frequency interval. When needed in further analysis we have fixed the value of ϵ_∞ to 1 for temperatures above 324 K. The fitted value of τ_2 is, however, still valid, although the maximum frequency is below the critical frequency [$\nu_c=1/(2\pi\tau_2)$]. We have tested this hypothesis at 331.1 K, where the critical frequency, ν_c, is 3.3 THz, by extending the frequency range with Zellsman's data[30] from 2 to 4.5 THz. This extension did not result in any change of the determination of τ_2. Kindt and Schmuttenmaer[17] have reported room-temperature relaxation times of 8.24 (40) ps and 0.18 (14) ps determined with THz-TDS in excellent agreement with our data at the same temperature.

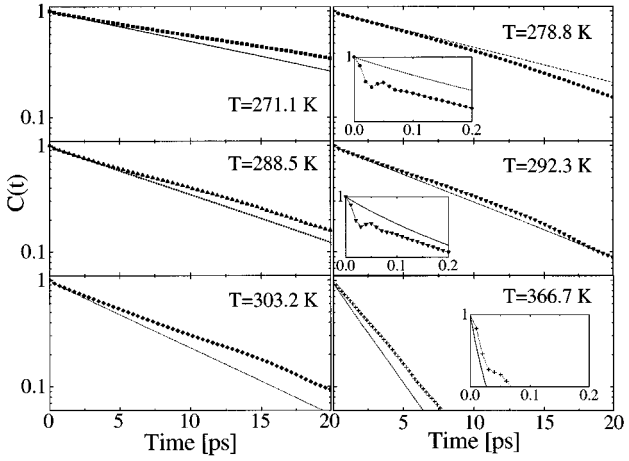

FIG. 8. The experimentally determined Debye correlation functions with two relaxation times [Eq. (11)] are represented by the lines. The molecular dynamics correlation functions are represented by the symbols. In the insert, the fast relaxation times are compared.

In the time domain, dielectric relaxation may be considered as the interaction between an external time-dependent field and the total dipole moment of the system, **M**. Applying perturbation theory, dielectric relaxation may be described with the normalized time correlation function of **M**[41]

$$C(t)=\frac{\langle\mathbf{M}(0)\cdot\mathbf{M}(t)\rangle}{\langle M^2\rangle}. \tag{10}$$

In the double Debye model, the correlation function, $C(t)$ is described by a biexponential decay, with amplitudes proportional to the differences $\epsilon_s-\epsilon_1$ and $\epsilon_1-\epsilon_\infty$

$$C(t)=\frac{\epsilon_s-\epsilon_1}{\epsilon_s-\epsilon_\infty}\,e^{-|t|/\tau_D}+\frac{\epsilon_1-\epsilon_\infty}{\epsilon_s-\epsilon_\infty}\,e^{-|t|/\tau_2}. \tag{11}$$

The time-correlation functions are plotted in Fig. 8.

V. MOLECULAR DYNAMICS SIMULATION

MD simulations of dielectric properties are properly carried out with the Ewald lattice summation method or the reaction field method.[42] The static dielectric constant may be calculated with the Ewald technique as[42]

$$\frac{4\pi\langle M^2\rangle}{3VT}=\epsilon_s-1, \tag{12}$$

where **M** is the dipole moment, V is the volume, and T the temperature of the simulation box. Dielectric properties have previously been calculated by adopting several different

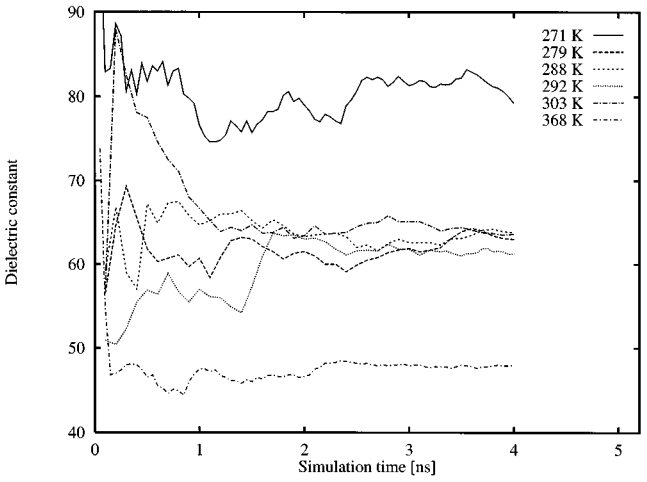

FIG. 9. The static dielectric constant found by MD simulations as a function of the simulation time.

model potentials,[26,43–47] but apart from the studies carried out by Neumann,[26,27] the simulation times extend to less than a ns.

We have carried out MD simulations at selected temperatures of the experimental spectra by adopting experimental densities and the SPC/E potential,[48] which is a reparameterization of the original SPC potential[49] to include also the self-energy polarization term. The reason for choosing the SPC/E potential is that it is both extremely simple (and thus efficient in these computer-demanding calculations), and that it has given reasonable results in previous work. The Ewald lattice summation technique and periodic boundary conditions have been employed, and we have not been using any spherical cutoff, but instead included all interactions in the simulation box.[46] The simulated system consists of 216 water molecules and the simulation time is 4 ns with a timestep of 2 fs.

The dielectric constant as a function of the simulation time is presented in Fig. 9. We conclude that simulation times of more than 2.0 ns are required to obtain a reasonable convergence. It is noted that at 303.2 K the static dielectric constant is 88 after 200 ps before reaching the final value of 63.6, and that at 292.2 K the static dielectric constant changes from 54 to 64 during the simulation period 1.4–1.7 ns. The slow convergence of the dielectric constant, which persists after many hundreds of picoseconds, has not been explained at a molecular level, but it is noted that they exist up to 1 ns at all temperatures. The standard deviation of the dielectric constant (Table II) is, however, substantially smaller at the highest temperature, 368.2 K than at lower temperatures. As noted for a flexible SPC potential,[43] it is clear that the slow convergence is due to a collective behavior of liquid water since the corresponding average of the molecular dipole moment, $\langle \mu^2 \rangle$, converges much more rapidly.

The temperature dependence of the static dielectric constant is compared with experimental values[50] in Fig. 10. Within the temperature interval 278–303 K, the correct temperature dependence is not obtained. This is probably due to the limited simulation times as noted both in Fig. 9 and Table II. If we had been interested in only the time-independent dielectric constant, sampling with an umbrella potential would improve the convergence of the dielectric constant.[51]

TABLE II. Parameters obtained by MD simulations with a simulation time of 4.0 ns. The standard deviation of the static dielectric constant, ϵ_s, is calculated by partitioning the simulation time into macrosteps of time t_m and regarding the average of each macrostep as an independent measurement. The Debye relaxation time, τ_D, is calculated with linear regression in the range τ_r.

T [K]	t_m [ps]	ϵ_s	τ_D [ps]	τ_r [ps]
271.05	20	79.2(3.0)	18.9(1.7)	0.5–29
278.75	10	63.0(1.8)	10.7(0.5)	0.5–22
288.45	10	63.8(1.8)	11.1(0.6)	0.5–22
292.15	10	61.3(2.0)	8.1(0.3)	0.5–22
303.15	10	63.6(1.8)	8.8(0.4)	0.5–22
368.15	5	48.0(0.9)	2.73(0.11)	0.5–8

The static dielectric constants from our simulations are generally too small compared with the experiment in Fig. 10. This may be understood from the fact that we use a rigid and nonpolarizable potential function. If an external electric field is applied to a liquid, mainly three things happen: The electronic charge distribution is polarized, the geometry of the molecule is altered, such as the molecular dipole moment is increased, and the water molecules are aligned. Here, we only include the third term. It has been demonstrated that many-body polarization has a large effect on the determination of dielectric properties,[52,53] but that a water molecule with an effective dipole moment of that in the liquid state has the same structural and dielectric properties as the fully polarizable system.[52] It is therefore expected that a large part of the deviations to experiment is due to the description of the collective orientational ordering of the water molecules. For example, it has been argued that the accuracy of the quadru-

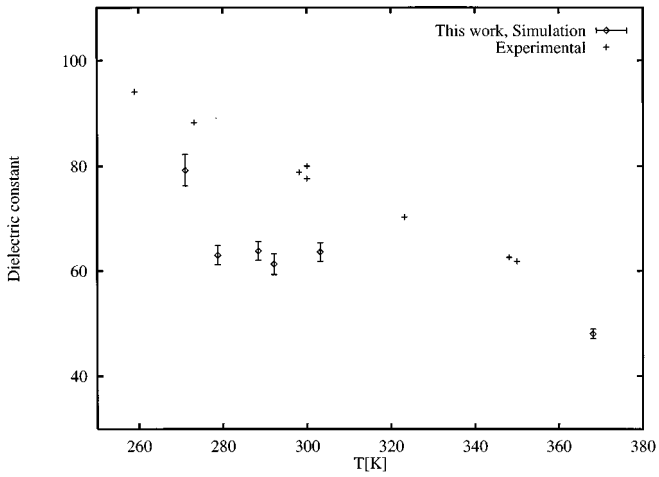

FIG. 10. The static dielectric constant found by MD simulations (diamond) as a function of the temperature. Experimental data (Ref. 50) (cross) are shown for comparison.

pole moment of the water molecule has a large influence on the dielectric constant since it effectively breaks the long-range dipole–dipole correlations.[52] Quantum chemical potentials that provide an accurate description of the true molecular charge distribution, such as the NEMO potential,[54,55] may thus give an improved description of dielectric properties of polar liquids. It may also be of importance that solvent effects on the molecular quadrupole moment is included. The high static dielectric constant is an exceptional property of liquid water, but it is important to remember that also other liquids such as formamide, ethylene carbonate and *N*-methylacetamide, which has a very different structure than that of water also have as high dielectric constants.[56]

Calculations of the dielectric relaxation as the time-correlation function in Eq. (12) should agree better with experiment than the dielectric constant. The reason is that the electronic polarization and the intramolecular motions occur on a different time scale than that considered here. On the other hand, couplings between the different kinds of polarizations may be important. In the Debye approximation the relaxation of the collective orientational motion is described with transition state theory, i.e., the relaxation occurs by passing an energy barrier. It is possible that the molecular induced dipole moment and the molecular geometry are different from the average values at the transition state, which of course will affect the height of the energy barrier and thereby also the relaxation time. The mechanism behind Debye relaxation may be regarded similar to that of self-diffusion because the energy barrier is in both cases due to the breaking and forming of hydrogen bonds.[57,58] For the SPC potential, it has been noted that a flexible potential reduces the self-diffusion coefficient significantly.[43]

In the Debye model, the dielectric relaxation is described with a single relaxation time, τ_D, as

$$C_D(t) = e^{-|t|/\tau_D}, \tag{13}$$

for t larger than ~ 0.5 ps. The calculated time-correlation functions are compared with our experiments in Fig. 8 and the times, τ_D, are given in Table II. The Debye time as a function of the simulation time is shown for some temperatures in Fig. 11. It is concluded that simulations of several hundreds of picoseconds are required to obtain a qualitatively correct behavior and of several ns to achieve a reasonable agreement with the experiment, even if the error bars are too large for establishing a relation for temperature dependence. The main point is, however, that in contrast to the dielectric constant, it is possible to obtain quantitatively correct Debye times with a rigid and nonpolarizable potential model.

VI. DISCUSSION

We have compared the temperature dependence of our Debye relaxation time, τ_D, with Debye relaxation times obtained from dielectric data in the microwave region,[36] τ_{MW} (Fig. 13). One would *a priori* expect the two times to be identical. This is the case at high temperatures, whereas at low temperatures τ_{MW} is higher than our measured τ_{D}. A possible explanation for this is a nonvanishing contribution from the fast relaxation process to the complex dielectric constant in the GHz region at low temperatures. At 278.8 K we find the fast relaxation time to be 0.26 ps, giving a critical frequency, ν_c, of 610 GHz. This gives a considerable contribution to the Debye spectrum in the entire GHz region. At higher temperatures the critical frequency will increase which decreases the spectral contribution at GHz frequencies from the fast relaxation process. At low temperature the microwave relaxation time, as observed by Kaatze and Uhlendorf,[36] will accordingly include contributions from the fast relaxation process, and is therefore different from our Debye relaxation time.

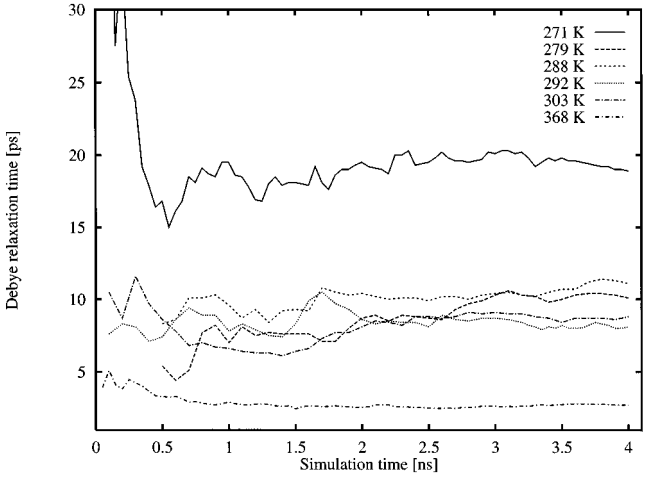

FIG. 11. The Debye relaxation time found by MD simulations as a function of the simulation time.

When we compare THz-TDS dynamics with the dynamics observed in TDFSS-experiments, it is important to realize that the TDFSS measurements probe the dynamical changes following a rapidly induced change in the charge distribution, whereas the experiments in this work probe the dynamics associated with a step-function change of the electric field.[59] In a dielectric model this distinction is equivalent to a longitudinal relaxation time (τ_L) associated with the charge change and a transverse relaxation time (τ_T) associated with the field change.[60] Following Kivelson and Friedman,[60,61] these two relaxation times are related through the dielectric constant at zero and ''infinite'' frequency, where infinite means $\omega \gg 1/\tau$

$$\tau_T = \tau_L \frac{\epsilon_s'}{\epsilon_\infty'}. \tag{14}$$

The TDFSS measurement of Jimenez *et al.* show a double exponential decay with time constants 120 and 880 fs at room temperature.[15] Using for the fast relaxation (120 fs) $\epsilon_s' = \epsilon_1$ and $\epsilon_\infty' = \epsilon_\infty$ we obtain a relaxation time of 195 fs in agreement with our measured $\tau_2 = 170$ fs at 292.3 K. For the slow component (880 fs) we obtain, using $\epsilon_s' = \epsilon_s$ and $\epsilon_\infty' = \epsilon_1$, a relaxation time of 12.8 ps in comparison with the measured $\tau_D = 8.5$ ps. Considering the simplicity of the model the observed agreement is good, as it was also ob-

served by Ohmine.[62] It should be noted that the relaxation times from the TDFSS experiment change less than a factor of 2 for different the solute molecules.[59] It is therefore reasonable to assume that the relaxation times mainly are determined by the same mechanisms as the dielectric relaxation times and very little affected by interactions (such as hydrogen bonds) between the solute and solvent.

In the work of Mizoguchi *et al.*[10] two Curie–Weiss equations are adopted for describing the temperature dependence of the DRS relaxation times (τ_{DRS}). We have used these to calculate τ_{DRS} at temperatures corresponding to ours (Fig. 12). The values of τ_{DRS} and τ_D differ as does their temperature dependence. The relaxational mode observed in the DRS-experiment depends on the dynamics of the nonlinear polarization, whereas the time dependence observed in our data results from the dynamics of the linear polarization. The two macroscopic properties do not necessarily couple equally to the different kinds of thermal fluctuation in the microscopic structure. The ratio of τ_D and τ_{DRS} is theoretically predicted to be three[63] for liquids dominated by single molecule rotational relaxation. We find that this ratio changes from 2.2 at 271.1 K to 1.3 at 366.7 K. It is not surprising that the ratio departs from three since collective effects are known to dominate both the FIR and DRS spectra. The reason for the change of the ratio with temperature is presently unknown, but the change could suggest a difference in the molecular mechanisms determining the two spectra.

Like the DRS-technique, the OHD-RIKES/OKE experiments depend on the nonlinear polarization. Castner *et al.*[13] suggest that due to the nature of their experiment the relaxation times of 0.40 and 1.16 ps at $T=295$ K can be directly assigned to rotational diffusion, although some translation diffusion may be included because of the hydrogen bond network. It would be interesting to have OHD-RIKES data over a larger temperature interval in order to perform a more detailed comparison.

In previous temperature-dependence studies of dielectric relaxation, several attempts have been made to account for the temperature dependence of the Debye relaxation. A procedure commonly employed is to make an Arrhenius plot and analyze it with transition state theory[64]

$$\tau(T)=\frac{h}{kT}\exp\left(-\frac{\Delta S_a}{R}\right)\exp\left(-\frac{\Delta H_a}{RT}\right)\equiv\frac{\tau_0}{T}\exp\left(-\frac{\Delta H_a}{RT}\right),\tag{15}$$

where ΔH_a is the activation enthalpy and ΔS_a is the activation entropy for the relaxation process. Both ΔH_a and ΔS_a are assumed to be temperature independent. The Debye relaxation time versus $1000/T$ is shown in Fig. 13. We find that a single constant activation enthalpy cannot fit the data appropriately over the entire temperature range, but this is possible if the data divided in two regions, one above 315 K and one below 293 K. The two lines intersect near 303 K. At high temperatures the activation enthalpy is 2.9 kcal/mol and at low it is 4.0 kcal/mol. It is interesting to note that 303 K has proven to be a special temperature in various studies of water. Mizoguchi *et al.* have plotted the inverse of the DRS relaxation time versus temperature[10] and observed a kinklike behavior at $\sim$303 K. In pressure dependent studies of the shear viscosity,[65] water behaves like an abnormal liquid below 303 K and the specific heat capacity of water, C_p, has a minimum at 303 K.[66] Temperature dependence of a property measured in one kind of experiment does not give a total picture of all thermal fluctuations. Still, adding all these observations together we obtain indication of a changes in microscopic structure at $\sim$303 K. In our case this is observed as a change of the energy barrier of the reorientation process.

The assumption that the activation enthalpy for the relaxation process is constant may not be valid. The temperature dependence of Arrhenius plots for kinetic properties may reflect a decreasing interaction energy as the tempera-

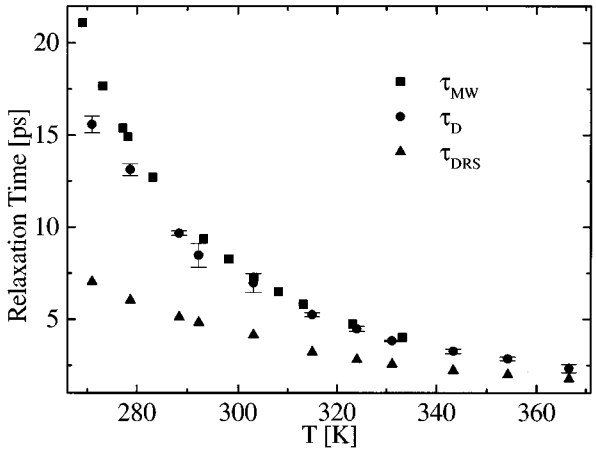

FIG. 12. The Debye relaxation times, τ_D, represented by circles are compared to: (a) Relaxation time from a temperature-dependent study of dielectric relaxation in the microwave region (Ref. 36) represented by squares, and (b) relaxation times from a temperature-dependent DRS study (Ref. 10) represented by upper triangles.

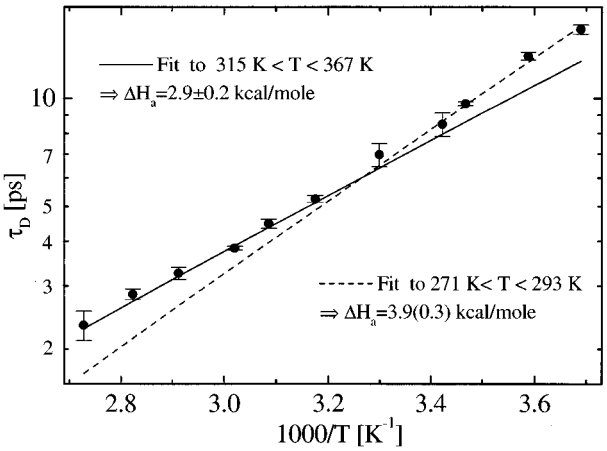

FIG. 13. The circles show the Debye relaxation times, τ_D, vs $1000/T$. The error bars indicate the 95% confidence limit. The solid and dashed lines are a transition state fit to the high- and low-temperature regions, respectively, yielding $\tau_D=\{[15(5)]/T\}\times e^{[1400(100)]/T}$ and $\tau_D=\{[3(1)]/T\}\times e^{[2000(200)]/T}$.

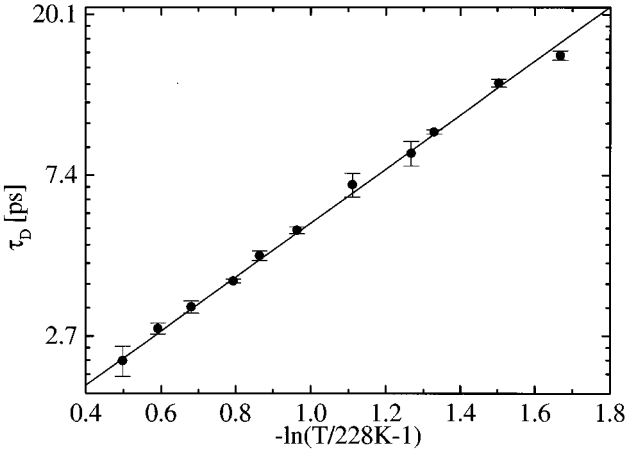

FIG. 14. The circles show the Debye relaxation times, τ_D, vs $-\ln(T/228-1)$. The linear fit, $\ln \tau_D = 1.68(0.03) \times + 0.02(0.03)$, shows the power dependence.

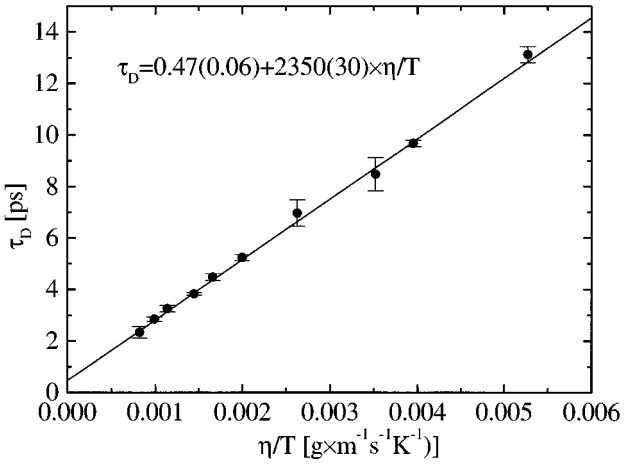

FIG. 15. The circles show the Debye relaxation time versus the shear viscosity (Refs. 50 and 75) divided by the temperature. The linear fit, $\tau_D = 0.47(0.06) + 2350(30)\ \eta/T$, shows the coefficient in the Debye–Stokes–Einstein relation.

ture increases (see for example Ref. 67). If the rate-determining step in the Debye relaxation process is the breaking and forming of hydrogen bonds, the temperature dependence may origin from a decrease in the number of hydrogen bonds with increasing temperature. Furthermore, since it has recently been demonstrated that the dynamics of forming and breaking hydrogen bonds at room temperature in liquid water is virtually uncorrelated with the fluctuations of neighboring bonds (i.e., cooperative effects are unimportant for the forming of a hydrogen bond in liquid water),[68] it may be possible to use a statistical model, where only the temperature dependence of the number of hydrogen bonds to each molecule models the properties of liquid water.[5,24,69] On the other hand, simulations using a polarizable potential model find cooperative effects in the hydrogen bonding of liquid water.[70] It is also reasonable that a major portion of the cooperative effect arises from a polarization of charge distribution when a hydrogen bond is formed. This effect is not included in an effective force field as the SPC/E potential, but on the other hand, effective pair potentials have successfully described many properties of liquid water, including diffusion coefficients and dielectric relaxation that depend on the dynamics of the forming and breaking of hydrogen bonds.

The possibility of a true singularity in both static and dynamic properties of liquid water at about $T_s = 228$ K (1 bar) has been suggested by Speedy and Angell.[25,71] This temperature is just below the limit of the attainable supercooling at about 232 K. It has been shown that the temperature dependence of experimentally measured properties that exhibit an extremum (e.g., isothermal compressibility, density, and NMR relaxation times)[71] may be fitted to a fractional power law that diverges to infinity at T_s. The same parameters are used for liquid water in the supercooled and the normal temperature regime. In the case of the Debye relaxation time the model has been found to resemble the actual behavior at temperatures between 273.2 and 333.2 K[71] giving the equation, $\tau_D = 0.9822[\text{ps}](T/T_s - 1)^{-1.791}$. A comparison of our $\ln \tau_D$ versus $-\ln(T/228-1)$ (Fig. 14) gives an excellent agreement with the findings of Speedy and Angell.[71] We find the exponent to be -1.68 ± 0.03 in comparison with -1.791 ± 0.02.[71] If it is a singularity at 228 K that governs the temperature dependence also in the normal temperature regime, it would be crucial for an MD simulation to model this behavior in order to describe the temperature dependence of liquid water in both the supercooled and normal temperature regime which for example has been problematic for the density.[72,73]

The Einstein–Stoke relations demonstrate that the Debye relaxation time, τ_D, the shear viscosity, η, and the self-diffusion coefficient are related and thereby should originate from the same molecular mechanisms.[57,58] The Debye–Einstein–Stoke model for the relation between η and τ_D, is given by[74]

$$\tau_D = 4\pi\eta R^3/k_B T, \tag{16}$$

where R is the hydrodynamic radius of a rotating molecule, T the absolute temperature, and k_B Boltzmann's constant. We have plotted our Debye relaxation time versus the shear viscosity[50,75] divided by temperature (Fig. 15) and we find a linear dependence.

Agmon has suggested that the Debye relaxation is caused by a tetrahedral displacement.[23] That would in terms of a lattice theory be a translation from one site to a neighboring site, a motion that also includes a rotation. Such a mechanism is consistent with the finding that about half of the water molecules in liquid water use only three of the four bonding sites[76] and the view that water is a random hydrogen-bonded network with frequently strained and broken bonds, continuously subject to spontaneous restructuring.[77] The tetrahedral displacement is also consistent with that the number of hydrogen bonds is sufficiently large for the water molecules to form an infinite connected network (''gel'').[77,78] Note that such a model is inconsistent

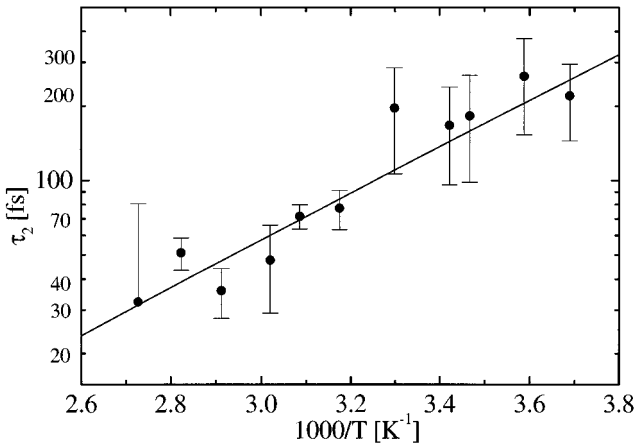

FIG. 16. The circles show the relaxation times, τ_2[fs], vs $1000/T$. The error bars indicate the 95% confidence limit. The solid line is a transition state fit yielding $\tau_2 = \{[70(70)]/T\} \times e^{[1900(300)]/T}$.

with the assumption that liquid water consists of two fractions of molecules with different hydrogen-bond properties.[79–83]

The temperature dependence of the fast relaxation time, τ_2, supports the assumption of two relaxational processes opposed to one relaxation process and one resonance. The temperature dependence of the frequency of maximum absorption for a relaxation process $(1/\tau_2)$ has the form of Eq. (15), while for a resonance process the temperature dependence of the frequency of maximum absorption is small.[5] τ_2 is plotted versus $1000/T$ in Fig. 16. The fast relaxation time changes by a factor of roughly 8 over the temperature range. Although there is a good deal of scatter, this change can be described by a transition state model. The fast relaxation process is also observed in the simulations (Fig. 8), but this is a region of the spectrum where quantum effects start to become important,[53] and such contributions have not been included here.

The amplitudes $A_D = \epsilon_s - \epsilon_1$ and $A_2 = \epsilon_1 - \epsilon_\infty$ are proportional to the contributions from the two relaxational modes to the macroscopic polarization. The temperature dependence therefore reflects changes in the microscopic structure that influence the mechanisms behind each relaxation process. In Fig. 17 the amplitudes from the experimental correlation function are plotted as a function of temperature (the static dielectric constant has been taken from Ref. 40). We find that the two modes do not contribute equally much. The Debye relaxation contributes of 94%–98.5%. The bandwidth of the THz pulses used in this study is not wide enough to determine either the static dielectric constant at any temperature or ϵ_∞ at temperatures above 324.1 K. However, if we assume that at temperatures lower than 324.1 K the temperature dependence of the amplitudes is not an artifact produced by a limited bandwidth, we observe that the contribution of the Debye relaxation to the macroscopic polarization decreases and contribution of the fast relaxation increases vaguely with increasing temperature. Following Agmon's model,[23] we can explain this temperature dependence of A_D

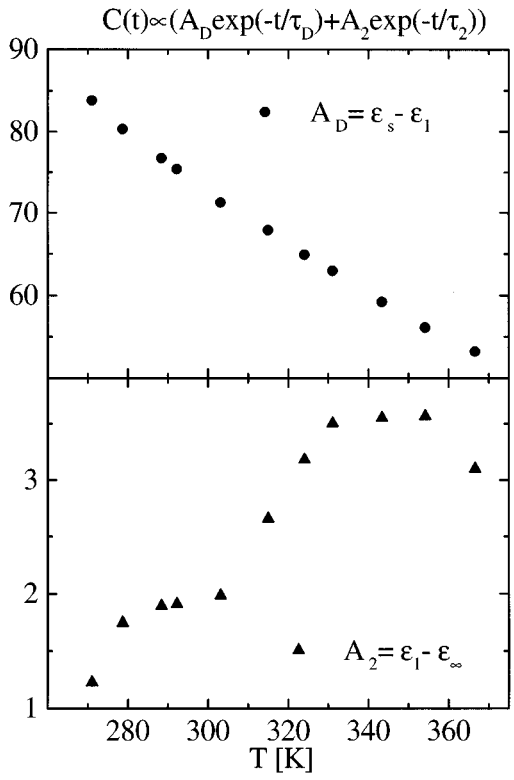

FIG. 17. The contribution to the macroscopic polarization of the two relaxation processes as a function of temperature.

and A_2 qualitatively. According to this model the fast relaxation time is caused by a single-molecule rotation and, as discussed, the Debye relaxation is due to a tetrahedral displacement. At higher temperatures the thermal energy will break some of the hydrogen bonds. Single-molecule rotations will accordingly increase in proportion, whereas the number of tetrahedral displacements will decrease. It is noted that both processes may occur with one hydrogen bond intact. When we explain the temperature dependence A_2, we have to consider that we have measured τ_2 at room temperature to be in the order of 0.2 ps, whereas single-molecule reorientation is generally assumed to be around 1 to 2 ps.[84,85]

VII. CONCLUSION

With the use of THz-TDS we have measured the real and imaginary part of the dielectric constant of liquid water in the far-infrared region from 0.1 to 2.0 THz in a temperature range from 271.1 to 366.7 K. The data was fitted to a double Debye model, giving a fast (fs) and a Debye (ps) relaxation time for the macroscopic polarization. The temperature dependence of the Debye relaxation time was analyzed using three models. We have learned from transition state theory that the activation enthalpy for the reorientation process is not constant over the entire temperature range. We find a linear dependence between the Debye relaxation time and the viscosity divided by temperature in excellent agreement with the predictions of the Debye–Stoke–Einstein relation. Finally, we find that the temperature dependence of

the Debye relaxation time can be accounted excellently for by a fractional power law that arises from a singularity of liquid water at 228 K.

We have also performed extensive MD simulations of liquid water with the use of a rigid and nonpolarizable potential model (SPC/E). We have calculated the static dielectric constant and the corresponding time-correlation function at selected temperatures and carefully tested the convergence of these simulations. We concluded that simulation times of more than 2 ns were required to obtain a reasonable convergence and agreement with the experimental Debye time. The main conclusion is that it is possible to obtain quantitatively correct Debye times with a rigid and nonpolarizable potential model.

In future projects it would be interesting to extend the frequency range to higher frequencies in order to ensure a precise determination of the fast relaxation time, the temperature dependence of A_2, and to investigate resonances and also to include quantum effects in the simulations. Isotope studies could give a better understanding of the mechanisms behind the relaxation processes. Both experimental and theoretical work on $D_2O(l)$ is on the way.

ACKNOWLEDGMENTS

We would like to thank Mark Maroncelli and Ole Faurskov Nielsen for useful comments. Also, we gratefully acknowledge the financial support of the Danish Natural Science Research Council.

[1] *Water: A Comprehensive Treatise*, edited by F. Franks (Plenum, New York, 1972–1981), Vols. 1–2.
[2] D. Eisenberg and W. Kauzmann, *The Structure and Properties of Water* (The Clarendon, Oxford, 1969).
[3] J. N. Murrell and A. D. Jenkins, *Properties of Liquids and Solutions*, 2nd ed. (Wiley, London, 1994).
[4] J. B. Hasted, *Aqueous Dielectrics* (Chapman and Hall, London, 1973).
[5] J. B. Hasted, in *Water: A Comprehensive Treatise*, edited by F. Franks (Plenum, New York, 1972), Vol. 1.
[6] J. Barthel and R. Buchner, Pure & Appl. Chem. **63**, 1473 (1991).
[7] P. Debye, Verh. dt. phys. Ges. **15**, 777 (1913).
[8] P. Debye, *Polar Molecules* (Chemical Catalog, New York, 1929).
[9] F. Sobron, F. Puebla, F. Rull, and O. F. Nielsen, Chem. Phys. Lett. **185**, 393 (1991).
[10] K. Mizoguchi, Y. Hori, and Y. Tominaga, J. Chem. Phys. **97**, 1961 (1992).
[11] Y. J. Chang and J. E. W. Castner, J. Chem. Phys. **99**, 7289 (1993).
[12] S. Palese, L. Schilling, R. J. D. Miller, P. R. Staver, and W. T. Lotshaw, J. Phys. Chem. **98**, 6308 (1994).
[13] J. E. W. Castner, Y. J. Chang, Y. C. Chu, and G. E. Walrafen, J. Chem. Phys. **102**, 653 (1995).
[14] W. Jarzeba, G. C. Walker, A. E. Johnson, M. A. Kahlow, and P. F. Barbara, J. Chem. Phys. **92**, 7039 (1988).
[15] R. Jimenez, G. R. Fleming, P. V. Kumar, and M. Maroncelli, Nature **369**, 471 (1994).
[16] L. Thrane, R. H. Jacobsen, P. U. Jepsen, and S. R. Keiding, Chem. Phys. Lett. **240**, 330 (1995).
[17] J. T. Kindt and C. A. Schmuttenmaer, J. Phys. Chem. **100**, 10373 (1996).
[18] P. R. Smith, D. H. Auston, and M. C. Nuss, IEEE J. Quantum Elec. **24**, 255 (1988).
[19] M. v. Exter, C. Fattinger, and D. R. Grischkowsky, Opt. Lett. **14**, 1128 (1989).
[20] D. R. Grischkowsky, S. R. Keiding, M. v. Exter, and C. Fattinger, J. Opt. Soc. Am. B **7**, 2006 (1990).
[21] J. E. Pedersen and S. R. Keiding, IEEE J. Quantum Electron. **28**, 2518 (1992).
[22] M. Vedamuthu, S. Singh, and G. W. Robinson, J. Phys. Chem. **100**, 3825 (1996).
[23] N. Agmon, J. Phys. Chem. **100**, 1072 (1996).
[24] H. E. Stanley and J. Teixeira, J. Chem. Phys. **73**, 3404 (1980).
[25] C. A. Angell, in *Water: A Comprehensive Treatise*, edited by F. Franks (Plenum, New York, 1981), Vol. 7.
[26] M. Neumann, J. Chem. Phys. **82**, 5663 (1985).
[27] M. Neumann, J. Chem. Phys. **85**, 1567 (1986).
[28] *Properties of Silicon* (INSPEC, The Institution of Electrical Engineers, London, 1988).
[29] G. Cocorullo and I. Rendina, Electron. Lett. **28**, 83 (1992).
[30] H. R. Zelsmann, J. Mol. Struct. **350**, 95 (1995).
[31] M. N. Afsar and J. B. Hasted, J. Opt. Soc. Am. **67**, 902 (1977).
[32] Z. Czumaj, Mol. Phys. **69**, 787 (1990).
[33] O. F. Nielsen, Annu. Rep. Prog. Chem. Sect. C, Phys. Chem. (Cambridge, 1993).
[34] M. N. Afsar and J. B. Hasted, Infrared Phys. **18**, 835 (1978).
[35] H. J. Liebe, G. A. Hufford, and T. Manabe, Int. J. Infrared Milimetre Waves **12**, 659 (1991).
[36] U. Kaatze and V. Uhlendorf, Z. Phys. Chem. NF **126**, 151 (1981).
[37] C. J. Montrose, J. A. Bucaro, J. Marshall-Coakley, and T. A. Litoritz, J. Chem. Phys. **60**, 5025 (1974).
[38] R. M. Hill, Nature **275**, 96 (1978).
[39] MicroMath® Scientist® for windows™, 2.01 ed. (MicroMath, Inc., 1986–1995).
[40] H. Zaghloul and H. A. Buckmaster, CJ. Phys. D: Appl. Phys. **18**, 2109 (1985).
[41] D. A. McQuarrie, *Statistical Mechanics* (Harper and Row, New York, 1976).
[42] M. Neumann, O. Steinhauser, and G. S. Pawley, Mol. Phys. **54**, 97 (1984).
[43] J. Andersen, J. J. Ullo, and S. Yip, J. Chem. Phys. **87**, 1726 (1987).
[44] H. E. Alper and R. M. Levy, J. Chem. Phys. **91**, 1242 (1989).
[45] K. Watanabe and M. L. Klein, Chem. Phys. **131**, 157 (1989).
[46] M. Belhadj, H. E. Alper, and R. M. Levy, Chem. Phys. Lett. **179**, 13 (1991).
[47] M. Souaille and J. C. Smith, Mol. Phys. **87**, 1333 (1996).
[48] H. J. C. Berendsen, J. R. Grigera, and T. P. Straatsma, J. Phys. Chem. **91**, 6269 (1987).
[49] H. J. C. Berendsen, J. P. M. Postma, W. F. v. Gunsteren, and J. Hermans, in *Intermolecular Forces*, edited by B. Pullman (Reidel, Dordrecht, 1981), p. 331.
[50] *Handbook of Chemistry and Physics*, 64th ed. (ERC, 1983–1984).
[51] Z. Kurtovic, M. Marchi, and D. Chandler, Mol. Phys. **78**, 1155 (1993).
[52] S. L. Carnie and G. N. Patey, Mol. Phys. **47**, 1129 (1982).
[53] B. Guillot, J. Chem. Phys. **95**, 1543 (1991).
[54] A. Wallqvist and G. Karlström, Chem. Scr. **29** A, 131 (1989).
[55] P.-O. Åstrand, P. Linse, and G. Karlström, Chem. Phys. **191**, 195 (1995).
[56] J. Padova, in *Water and Aqueous Solutions*, edited by R. A. Horne (Wiley-Interscience, New York, 1972).
[57] J. H. Wang, J. Chem. Phys. **69**, 4412 (1953).
[58] J. H. Wang, C. V. Robinson, and I. S. Edelman, J. Am. Chem. Soc. **75**, 466 (1953).
[59] M. Maroncelli, J. MacInnis, and G. R. Fleming, Science **243**, 1674 (1989).
[60] D. Kivelson and H. Friedman, J. Phys. Chem. **93**, 7026 (1989).
[61] H. L. Friedman, J. Chem. Soc. Faraday Trans. II **79**, 1465 (1983).
[62] I. Ohmine, J. Phys. Chem. **99**, 6767 (1995).
[63] R. M. Lynden-Bell and W. A. Steele, J. Phys. Chem. **88**, 6514 (1984).
[64] S. Glasstone, K. J. Laidler, and H. Eyring, *The Theory of Rate Processes* (McGraw-Hill, New York, 1941).
[65] J. C. M. Davis and J. Jarzynski, in *Water; A Comprehensive Treatise*, edited by F. Franks (Plenum, New York, 1972), Vol. 1.
[66] *Recommended Reference Materials for the Realization of Physicochemical Properties* (Blackwell Scientific, Oxford, 1987).
[67] F. H. Stillinger, Adv. Chem. Phys. **31**, 1 (1975).
[68] A. Luzar and D. Chandler, Phys. Rev. Lett. **76**, 928 (1996).
[69] G. H. Haggis, J. B. Hasted, and T. J. Buchanan, J. Chem. Phys. **20**, 1452 (1952).
[70] P. Barnes, J. L. Finney, J. D. Nicholas, and J. E. Quinn, Nature **282**, 459 (1979).
[71] R. J. Speedy and C. A. Angell, J. Chem. Phys. **65**, 851 (1976).
[72] S. R. Billeter, P. M. King, and W. F. v. Gunsteren, J. Chem. Phys. **100**, 6692 (1994).

[73] A. Wallqvist and P.-O. Åstrand, J. Chem. Phys. **102**, 6559 (1995).
[74] G. R. Flemming, *Chemical Applications of Ultrafast Spectroscopy* (Oxford University Press, New York, 1986).
[75] R. C. Hardy and R. L. Cottington, J. Res. NBS **42**, 573 (1949).
[76] A. Luzar and D. Chandler, J. Chem. Phys. **93**, 2545 (1993).
[77] F. H. Stillinger, Science **209**, 451 (1980).
[78] A. Geiger, F. H. Stillinger, and A. Rahman, J. Chem. Phys. **70**, 4185 (1979).
[79] H. S. Frank and W.-Y. Wen, Discuss. Faraday Soc. **24**, 133 (1957).
[80] G. Némethy and H. A. Scheraga, J. Chem. Phys. **36**, 3382 (1962).
[81] H. S. Frank, Science **169**, 635 (1970).
[82] V. I. Gaiduk, T. A. Novskova, and V. V. Brekhovskikh, J. Chem. Soc. Faraday Trans. **89**, 1975 (1993).
[83] Y. Maréchal, in *Hydrogen Bond Networks*, edited by M.-C. Bellissent-Funel and J. C. Dore (Kluwer, Dordrecht, 1994).
[84] C. M. Davis and J. Jarzynski, in *Water and Aqueous Solutions: Structure, Dynamics and Transport Processes*, edited by R. A. Horne (Wiley, New York, 1972).
[85] S.-H. Chen and J. Teixeira, Adv. Chem. Phys. **64**, 1 (1986).
[86] D. Bertolini, M. Cassettari, and G. Salvetti, J. Chem. Phys. **76**, 3285 (1982).
[87] O. F. Nielsen, Chem. Phys. Lett. **60**, 515 (1979).